Available online at www.sciencedirect.com
ScienceDirect
Polymer 47 (2006) 7259–7270
polymer
www.elsevier.com/locate/polymer

Quasi-static and hydrodynamic interaction between solid surfaces in polyisoprene studied by atomic force microscopy

Rüdiger Stark, Elmar Bonaccurso, Michael Kappl, Hans-Jürgen Butt*

Max-Planck-Institute for Polymer Research, Ackermannweg 10, 55128 Mainz, Germany

Received 22 May 2006; received in revised form 7 June 2006; accepted 8 June 2006
Available online 28 July 2006

Abstract

Forces across polymer melts are poorly understood despite their importance for adhesion and the structure of composite materials. Using an atomic force microscope (AFM) this interaction was measured for 1,4-polyisoprene (PI, $M_W = 1.9-10.2$ kDa). Weak repulsive forces which decayed with characteristic decay lengths of 0.4–1 nm were observed on silicon wafers, HOPG, and mica. This indicates that, unlike poly(dimethylsiloxane) (PDMS), PI does not form an immobilized layer. The results confirm theoretical predictions that no long-range force exist across polymer melts in thermodynamic equilibrium. In addition to quasi-static experiments (with microfabricated silicon nitride tips at low approaching velocity), hydrodynamic experiments (with attached glass microspheres as probes at high approaching velocity) were carried out with PI and PDMS ($M_W = 5.9$, 8.0, 18.8 kDa). In some cases slip was observed. Slip was correlated with the quasi-static forces: weak quasi-static forces (observed with PI and short-chain PDMS) were correlated with slip in hydrodynamic experiments, while strong repulsive forces observed with long-chain PDMS are correlated with the absence of slip.

Keywords: AFM; Polymer; Slip

1. Introduction

The interaction between solid surfaces across a polymer melt is studied for various reasons. First, knowledge about the interaction is important for dispersing particles in polymer melts, for example when making composite materials. Repulsive forces lead to an efficient dispersion while attractive forces tend to aggregate the particles. This becomes more and more relevant since current interest is in embedding nanoscopic inorganic particles. Second, it is of fundamental importance to understand the effect of confinement on polymers. Third, the interaction contains information on the structure and properties of the polymer at solid surfaces in general.

For these reasons the interaction between two solid surfaces across a polymer melt has been studied theoretically [1–5], in simulations [6,7] and experimentally. Most experiments were carried out with the surface forces apparatus (SFA). In the SFA the force between two crossed mica cylinders is measured versus distance. Different polymers such as poly(dimethylsiloxane) (PDMS) [8,9], perfluorinated polyether [10–13], polybutadiene (PB) [14,15], polyisoprene [16], and poly(phenylmethylsiloxane) (PPMS) [9,17–19] have been used. In all cases a rubber-like, non-flowing polymer layer of typically 1–3 times the radius of gyration R_g is observed. It effectively forms a hard wall. The molecular structure of the immobilized layer is not clear. Polymer chains can be pinned to an adsorbing surface not only directly by binding at several adsorption sites but also indirectly through their connection through the chain to other segments that themselves are adsorbed [1,18]. Beyond this immobilized layer the two interacting surfaces experience a long-range repulsion across PPMS [18], PB [15], and perfluorinated polyethers [10,13], which typically spans another 1–3 R_g. With PDMS an oscillatory, exponentially decaying interaction is observed [20,21].

* Corresponding author. Tel.: +49 6131 379 111; fax: +49 6131 379 310.
E-mail address: butt@mpip-mainz.mpg.de (H.-J. Butt).

0032-3861/$ - see front matter © 2006 Elsevier Ltd. All rights reserved.
doi:10.1016/j.polymer.2006.06.064

The oscillation period of 0.7 nm is equal to the diameter of the PDMS chain.

Recently we started to analyze the interaction of solid surface across polymer melts with the AFM [22–24]. Such experiments complement SFA measurements and probe the polymer melt under a different boundary condition. The reason is that the interacting areas are much smaller. In the SFA the interaction between two mica cylinders of $\approx$1 cm radius is measured while in the AFM a tip with a radius of curvature of typically 50 nm interacts with a planar surface. As a result of the small contact area and of the fact that radial pressure gradients are higher in the AFM, the polymer melt has a chance to escape underneath the approaching tip.

Results obtained with the SFA partially agree and in other parts disagree with AFM results. In recent AFM experiments [22–24] PDMS of different molecular weights, poly(ethylmethylsiloxane) (PEMS), and a diblock copolymer (PDMS-*b*-PEMS) was studied. The selected solid surfaces interacted strongly with the polymer, leading to small contact angles ($\Theta < 10°$). In agreement with earlier results [12,18,25–27] all experiments showed that polymers with the molecular weight above the entanglement molecular weight of $M_e =$ 12 kDa [28] showed repulsive forces, indicating the presence of an immobilized ''pinned'' layer. In contrast to SFA experiments low molecular weight PDMS led to attractive forces [23,24]. This is an indication that entanglement is required to stabilize the immobilized layer. In some cases, for example for PEMS on graphite, exponentially decaying oscillatory forces were detected [24].

Based on SFA and AFM experiments three relevant processes occurring at different time scales can be distinguished for polymers with a strong polymer–wall interaction: (1) Relaxation of individual chains, which is much faster than 1 s and which is achieved in SFA and AFM experiments. (2) Flow of the polymer into and out of the closing gap to establish equilibrium with a reservoir. The term ''restricted equilibrium'' was applied to characterize processes in which the chains can relax but the flow is too slow to equilibrate the gap with the reservoir [29,30]. This hydrodynamic process depends very much on the geometry. In AFM experiments with microfabricated tips the polymer melt can easily flow in and out of the gap. SFA experiments probe more the restricted equilibrium [8,15]. In this paper we show first experiments with the colloidal probe technique in which it is possible to choose the boundary condition by selecting an appropriate approaching velocity [3]. Formation of an immobilized layer in close vicinity to the solid surface. The corresponding time constant depends critically on the molecular weight of the polymer and the formation may take many hours [27,31,32]. Even in AFM experiments with microfabricated tips equilibrium is usually not obtained with respect to this process. The AFM results indicate that polymers with low molecular weight do not from such a layer.

All AFM experiments were carried out with polysiloxanes. In this paper we present results of AFM force measurements across PI with molecular weights below and above the entanglement molecular weight of 6.2 kDa [28]. PI interacts moderately strongly with the solid surfaces used, which is demonstrated by a contact angle of 7–27°. Until now to our knowledge all AFM experiments on polymer melts were carried out in a quasi-static mode, where microfabricated tips were used and the approaching velocity was so slow that hydrodynamic effects were negligible [23,24]. In this paper we describe hydrodynamic AFM experiments on polymer melts. The difference between ''quasi-static'' and hydrodynamic experiments is that instead of the microfabricated tip a spherical particle was used as probe and that the approaching velocity of the sphere to the surface was higher. As a result, the hydrodynamic force dominates over all other surface forces. Such experiments provide additional information about the viscosity of the confined polymer melt and about the hydrodynamic boundary condition, namely slip or no slip. A hydrodynamic boundary condition that describes slippage is $v_S = b \cdot dv_x/dz$. Here, v_S is the slip velocity, dv_x/dz is the local shear rate at the surface (x is the direction of the flow, z is directed normal to the surface), and b is the slip length. The slip length is the distance behind the interface at which the liquid velocity extrapolates to zero. Until now conflicting results have been reported. Flow experiments indicate that polymer melts and solutions show slip [33–41]. Slippage occurs either at the wall–polymer interface or few molecular layers away from the interface due to disentanglement within the polymer melt [42–46]. Slip is also observed in rheological measurements on polymeric dispersions of silica particles [47]. Dynamic force experiments with the SFA indicate either no change in viscosity or an increased viscosity of confined polymer melts which increases as the gap size decreases until at a certain distance a glass- or rubber-like layer is encountered [9,10,12,15,20]. The shear plane is always above the glass- or rubber-like layer and no slip is observed. NMR experiments of dispersions of solid particles in polymer melts [48,49] and dielectric spectroscopic measurements of confined PDMS [50] also show that relaxation times are slowed down near interfaces and in confinement.

2. Materials and methods

1,4-Polyisoprene was synthesized from isoprene by anionic polymerization. The isoprene was dissolved in freshly distilled cyclohexane and *sec*-butyl-lithium was added as a starter. After 12 h, the reaction was stopped with methanol and the product was recrystallized in tetrahydrofurane. The purity of the polymer was verified using gel permeation chromatography (GPC). The ratio of *cis* to *trans* was 70:30 as determined by NMR spectroscopy. By adjusting the amount of starter, PIs with molecular weights of $M_W = 1.9–10.2$ kDa were synthesized (Table 1). This corresponds to mean end-to-end distances of 3–8 nm. To avoid oxidation, PI was stored in light-protected flasks and at −8 °C. No change in the measured force curves for more than 16 h was observed. The oxidation in the AFM during measurements is therefore negligible. Additionally a GPC was measured of samples that were older than two years. These samples showed no oxidation.

Table 1
Molecular weights M_W, index of polydispersity M_W/M_n, and measured viscosity at 28 °C of polymers used

M_W/kDa	M_W/M_n	Viscosity/Pa s	R_0/nm
PI 1.9	1.15		3.3
2.5	1.10	0.68	3.8
4.8	1.08	1.64	5.3
6.8	1.06	2.94	6.3
8.0	1.06	4.31	6.9
10.2	1.04	7.70	7.8
PDMS 5.9	1.38	0.052	5.0
8.4	1.06	0.089	5.9
18.8	1.05	0.360	8.9

Values for the mean end-to-end distance R_0 were calculated from $R_0 = \sqrt{0.59 \cdot M_W}$ Å for PI and $R_0 = \sqrt{0.42 \cdot M_W}$ Å for PDMS [28].

Polydimethylsiloxane (PDMS) was synthesized from the trimer hexamethylcyclotrisiloxane by an anionic ring-opening polymerization. Ten percent of the monomer was dissolved in freshly distilled cyclohexane and *sec*-butyl-lithium was added as a starter. After 10 h, the rest of the monomer was added in a THF/cyclohexane mixture (60:40). The product was purified with a fractionator. To keep the polymers water free, all samples were stored under vacuum and on molecular sieves.

Viscosity was measured with an ARES system (Advanced Rheometric Expansion System, TA Instruments, Alzenau, Germany) with a steady shear measurement using two parallel plates at different shear rates ranging from 1 to 1000 s^{-1}, depending on the viscosity (Table 1). In the range of the shear rates of the instrument, the viscosities of all polymers were constant.

As *samples* we used muscovite mica (Plano GmbH, Wetzlar, Germany), silicon wafer with a natural oxide layer {100} (Si-mat Silicon Materials, Landsberg, Germany), and HOPG (highly oriented pyrolytic graphite, SPI Supplies, West Chests, PA). HOPG and mica were cleaved, the silicon wafer was plasma cleaned for 5 min at 30 W in an argon atmosphere of 0.1–1 mbar before each measurement.

Contact angles were measured for 2.0 and 10.2 kDa PI on different surfaces (Table 2) in the sessile drop configuration with a commercial contact angle measuring system (DSA 10, Krüss GmbH, Hamburg, Germany). The receding contact angles were <5° and too low to allow for a precise measurement. PDMS spreads on mica and silicon oxide and the contact angle is zero. It forms a small but finite advancing contact angle of ≈2° on HOPG.

Quasi-static force measurement: Before starting with force measurements, the sample was mounted onto the piezoelectric AFM scanner (Nanoscope 3 Multimode, Veeco Instruments, Santa Barbara, CA). Then, the AFM head with the liquid cell without O-ring and the cantilever were mounted, and the liquid cell was filled with polymer melt. The system was allowed to equilibrate with the laser turned on, and force measurements were started after at least 10 h. The temperature of the cell was around 28 °C, which was 4 °C above room temperature, and this heating was caused by the laser and the AFM electronics. During a force measurement the sample was periodically moved up and down at constant driving velocity v_0 by applying a voltage to the piezo translator while the cantilever deflection was measured. The result of such a measure is a plot of cantilever deflection versus position of the piezoelectric translator. From this a force-versus-distance curve, briefly called "force curve", was calculated by multiplying the cantilever deflection with the spring constant to obtain the force, and subtracting the cantilever deflection from the position of the piezo to obtain the distance. Figures typically show 10–30 force curves plotted together to allow for a visual averaging and to be able to estimate the noise level. Approaching velocities in static force experiments were 10–50 nm/s, if not otherwise mentioned.

Table 2
Advancing contact angles of 2.3 and 10 kDa polyisoprene on different surfaces

	Contact angle		
	Mica	HOPG	Silicon oxide
2.5 kDa	25°	7°	14°
10.2 kDa	27°	13°	20°

V-shaped cantilevers with silicon nitride tips (length 120 μm, width of each arm 18 μm, thickness 0.6 μm, Veeco Instruments, Santa Barbara, CA) were used. They were cleaned in a plasma cleaner for 5 min at 30 W with an argon atmosphere of 0.1–1 mbar before each measurement. The radius of the tip curvature was determined from scanning electron microscope (SEM) images (LEO 1530 Gemini, Oberkochen, Germany). A circle was fitted in the picture and the radius calculated from the scale of the image. Typical radii of curvature were between $R = 20$ and 100 nm. Cantilever spring constants were individually determined by the thermal noise method [51,52] with a Molecular Force Probe (MFP-1D, Asylum Research, Santa Barbara, CA). Spring constants ranged from 0.2 to 0.6 N/m. For each experiment a new cantilever was used to avoid contamination with polymer of the previous experiment.

Hydrodynamic measurements: To measure the hydrodynamic forces, the experimental setup was largely similar to the earlier described static force measurements, except for two changes. First, a particle (borosilicate glass microspheres, 20 μm nominal diameter, Duke Scientific Cooperation, Palo Alto, CA) was attached to a cantilever using epoxy resin (Epikote 1004, Shell, Germany). The radii of the particles were precisely determined after each experiment with the SEM and ranged from 9 to 11 μm. Second, the force curves were measured with much higher velocity, ranging from 200 nm/s to 100 μm/s. Spring constants measured after attaching the particle did not change significantly and were still in the range 0.2–0.6 N/m.

Analysis of hydrodynamic force curves: Experimental results were fitted with results of simulations. The hydrodynamic force curves are simulated solving the equation of motion for a sphere moving toward − or retracting from − a plane in a fluid:

$$F_h + F_{vdW} + F_c + F_{drag} = m^* \frac{d^2 D}{dt^2} \quad (1)$$

Here, D is the separation between sphere and flat surface, F_h is the hydrodynamic force, F_{vdW} is the van der Waals attraction, F_c is the restoring force of the cantilever, F_{drag} is the hydrodynamic drag on the cantilever, and m^*d^2D/dt^2 takes a possible contribution of acceleration into account. Since our system is characterized by small Reynolds numbers ($Re \ll 1$) the acceleration term can be neglected and was not further considered.

The effect of the hydrodynamic force is to retard the sphere and to alter the separation at a given time t compared to the movement of the piezo, which is driven at a constant velocity v_0. This results in a non-uniform velocity of the sphere dD/dt during the approach–retraction cycle. If a non-slip condition is assured, a hydrodynamic force of [53,54]

$$F_h = -\frac{6\pi\eta R^2}{D}\frac{dD}{dt} \tag{2}$$

is expected. Here, η is the viscosity of the liquid, R is the radius of the sphere, D is the separation between sphere and flat surface and dD/dt is the relative velocity of the two approaching surfaces. The negative sign arises because the force is directed opposite to the motion of the sphere.

Vinogradova [55] extended these calculations and introduced a correction factor f^*, which takes surface slip into account, assuming that both surfaces show the same slipping behavior:

$$F_h = -\frac{6\pi\eta R^2}{D}\frac{dD}{dt}\cdot f^*, \quad f^* = \frac{D}{3b}\cdot\left[\left(1+\frac{D}{6b}\right)\cdot\ln\left(1+\frac{6b}{D}\right)-1\right] \tag{3}$$

Here, b is the slip length. It is a fitting parameter and is not measurable a priori, while all other parameters in Eqs. (2) and (3) can be independently determined from further measurements. Both models ('no slip' and 'slip') assume creeping flow (low Reynolds number), Newtonian fluids, and small distances ($D \ll R$).

Van der Waals interactions were expressed as

$$F_{vdW} = -\frac{A_H R}{6D^2} \tag{4}$$

where A_H is the Hamaker constant. The negative sign indicates that the force is attractive and directed downward. We used a Hamaker constant of $A_H = 2\times10^{-21}$ J, which was estimated for interaction of glass and silicon oxide over polymer melt using the refractive indices n, the dielectric constant ε, and the electronic absorption frequency ν_e. (glass: $n = 1.47$, $\varepsilon = 4.6$, $\nu_e = 3.2\times10^{15}\ s^{-1}$; silicon oxide: $n = 1.45$, $\varepsilon = 3.82$, $\nu_e = 3.2\times10^{15}\ s^{-1}$; polymer melt: $n = 1.405$, $\varepsilon = 3.99$, $\nu_e = 2.8\times10^{15}\ s^{-1}$). The van der Waals forces turn out to be small or even negligible compared to typical hydrodynamic forces measured here. To be on the safe and accurate side we nevertheless included them in the calculation.

The restoring force of the cantilever spring was expressed by

$$F_c = k_c(D - D_0 - v_0 t) \tag{5}$$

where k_c is the spring constant of the cantilever and D_0 is the initial (at $t = 0$) separation between sphere and plane.

Finally, there is a contribution of the viscous drag on the cantilever. The viscous drag increases nearly linearly with the velocity of the cantilever. If the radius of the sphere is large enough, which in our case means approximately $R > 8$ μm [56], the drag on the cantilever may be considered as a constant contribution F_{drag}. This finally led to

$$F_h + F_{vdW} + F_c + F_{drag} = 0 \tag{6}$$

Combining Eqs. (2)–(6) yields a system of two equations of motion, one for the approaching, one for the retracting part:

$$-\frac{6\pi\eta R^2}{D}\cdot\frac{dD}{dt}f^* - \frac{AR}{6D^2} + F_{drag} = \begin{cases} k_c(D - D_a + v_0 t) & \text{for } 0 < t \le t_a \\ k_c(D - D_r - v_0 t) & \text{for } t_a < t \le t_r \end{cases} \tag{7}$$

Here, D_a and D_r are the initial separations of the sphere and the plane, respectively for approach and retraction, while t_a and t_r are the approach and retraction times. The initial conditions are

$$\begin{cases} D(t=0) = D_a & \text{for } 0 < t \le t_a \\ D(t=t_a) = D_r = 0 & \text{for } t_a < t \le t_r \end{cases} \tag{8}$$

The above differential equations cannot be solved analytically. A numerical solution was implemented in Maple V (Waterloo Maple Inc., Ontario, Canada).

3. Results and discussion

3.1. Quasi-static experiments with microfabricated tips

Weak, short-ranged repulsive forces were observed on silicon wafers for all molecular weights. As one example, a normalized force curve is shown in Fig. 1. Compared to earlier results obtained with PDMS [22–24] the repulsion was shorter ranged and weaker (Fig. 1B). Differences between molecular weights were not pronounced; we observed only a tendency of the repulsion to become weaker and shorter ranged with increasing molecular weight. For a quantitative comparison, normalized force curves were fitted with an exponential function according to $F = A_0 e^{-D/\lambda}$. Here, F is the measured force, λ is the decay length, and A_0 is a prefactor. Decay lengths were typically 0.8–1.0 nm at $M_W = 1.9$ kDa and decreased to 0.3–0.6 nm for 6.8 kDa. At higher molecular weight, in particular at $M_W = 10.2$ kDa, the repulsive force was often almost undetectable.

Forces on HOPG and mica were likewise repulsive and they showed similar decay lengths, though they were consistently weaker by a factors of 2 to 3 then on silicon oxide (Fig. 2), although the contact angle of PI on HOPG is lower than on a silicon oxide, and, on mica is larger than on silicon oxide.

The results confirm theoretical considerations of de Gennes [1] and Ausserré [2], lattice model-based computer

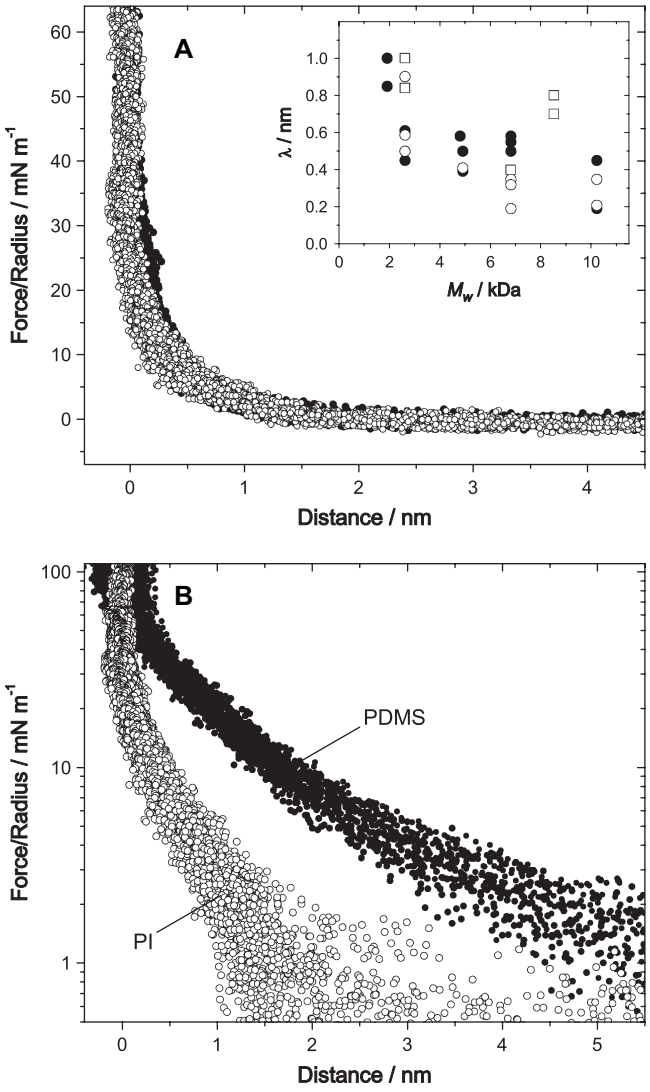

Fig. 1. A: Force curves measured in PI ($M_W = 2.5$ kDa) on a silicon wafer with a silicon nitride tip. Approach (●) and retraction (○) are shown. Thirty one force curves are superimposed to allow for a "visual" averaging. Forces were normalized by dividing them by the radius of curvature of the tip ($R = 70$ nm). Approaching and retracting force curves were calibrated separately to get rid of the constant (not distance dependent) viscous drag of the cantilever. The inset shows the decay lengths λ obtained when fitting the curves with an exponential function $F = A_0\exp(-D/\lambda)$. Decay lengths determined from experiments on silicon wafers (●), HOPG (○), and mica (□) are plotted. B: Normalized force curves measured in PI in logarithmic scale compared to force curves measured in PDMS ($M_W = 18$ kDa) on silicon oxide. Only the approaching parts are displayed.

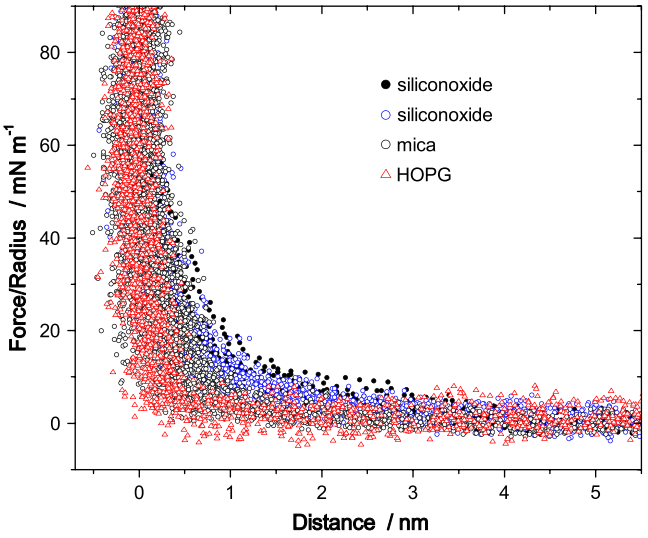

Fig. 2. Normalized force curves measured on a silicon wafer, on mica ($R = 80$ nm), and on HOPG ($R = 40$ nm) in polyisoprene with $M_W = 6.8$ kDa. For silicon oxide the results of the two experiments ($R = 25$ and 30 nm) are plotted.

simulations [6] and self-consistent field theories [5]. All authors predicted that in perfect thermodynamic equilibrium long flexible chains in a melt should not generate long-range interactions between two solid plates. Only if the chains are pinned at the surfaces an interaction in the range of the radius of gyration should exist. In our case the forces are so low that pinning does not seem to be significant.

This is in contrast to previous results obtained with PDMS. With PDMS a weak attraction was observed at $M_W < M_e$ (=12.0 kDa). For $M_W > M_e$ the force was strongly repulsive. This was attributed to the formation of an immobilized layer. Polymer molecules in direct contact with the solid interface were not able to equilibrate with the bulk polymer on the time scale of an AFM force experiment. At this point it is appropriate to discuss the structure of the immobilized layer. We attribute its formation to the adsorption of the PDMS at individual adsorption sites on the surface. This adsorption is reversible but slow, so that within the time span of one contact between the AFM tip and the surface it cannot equilibrate. We would also like to mention that in addition of adsorption/desorption of individual bonds a lateral movement of bonds might be possible. The activation barrier with respect to lateral diffusion might be much lower than that for desorption, in particular on homogeneous surfaces such as mica. Adsorbed chains, which have at least two adsorption sites entangle other chains. This leads to an enhanced entanglement, not because of an increased entanglement of chains with each other but due to the presence of the adsorbing surface. The polymer chains which at a given time are adsorbed at the surface still assume a random coil configuration and are not stretched away from the surface. Upon approach of the tip the adsorbed or "pinned" chains are compressed, which leads to a repulsive force. The absence of a repulsion in experiments with PI indicates that no immobilized layer is formed. We take this as evidence that PI segments do not adsorb either so strongly, or that their binding/debinding rate is much faster, or that the binding sites can easily move laterally on the surface.

We called the experiments described above "quasi-static" experiments because the results were independent on the approaching/retracting velocities and we assume that viscous drag had no influence on calibrated approaching force curves. There is one restriction, which is not relevant with respect to confined polymers, but with respect to the technique of AFM force measurements. In many experiments we observed an apparent strong repulsion in the retracting parts of force

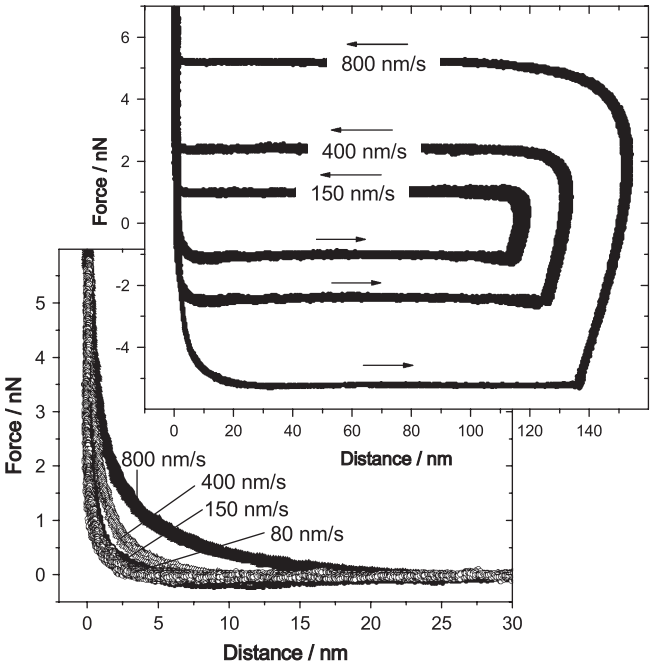

Fig. 3. Complete force cycles including the approach and retracting part without calibrating the force to zero but including a calibration with respect to distance. The experiment was carried out with 4.8 kDa PI on a silicon wafer using a V-shaped silicon nitride cantilever with a spring constant of 0.20 N/m. At the bottom left retracting, fully calibrated force curves measured with retracting velocities of 80 (○), 150 (●), 400 (△), and 800 nm/s (▲) are plotted.

curves (Fig. 3). This repulsion increased with retracting velocity. We attribute this to the hydrodynamic drag on the cantilever. When the cantilever is retracted the tip is still in contact with the sample surface. Thus, the velocity of the tip is zero, while the back of the cantilever is already moving with its constant retracting velocity v_0. Only when the tip is released from the surface the end of the cantilever starts to move. Due to the damping of the viscous liquid it reaches its final retracting velocity v_0 only after a delay. This implies, that the hydrodynamic force on the cantilever is not constant, but it increases with time. Since in the calibration the hydrodynamic drag on the cantilever is assumed to be a constant, this effect is not taken into account. It leads to an apparent repulsion if the viscous drag exceeds a certain value. The effect is proportional to $v_0\eta$. To avoid this effect the calibration procedure for retracting force curves is only allowed for $v_0\eta \ll 10^{-7}$ N/m.

3.2. Hydrodynamic experiments with microspheres

3.2.1. Polyisoprene

Force curves measured with microspheres showed a long-range repulsive force, which decreased with distance, plus a constant, distance-independent component (Fig. 4). The distance-independent component is caused by the drag on the cantilever. The long-range decaying force is due to the fact that the polymer melt has to be squeezed out of the closing gap between planar surface and microsphere. Both components increased with the approaching velocity v_0 and with the viscosity of the melt. For a quantitative interpretation force curves were fitted without slip and including slip. If slip is not present, the force curve should show a smooth transition when the particle contacts the surface, whereas if slip is present, the transition is abrupt and results in a kink at zero distance. Since small slip lengths (small kinks) are difficult to observe in force curves, we additionally discuss velocity-versus-distance curves or briefly "velocity curves". The transition from polymer melt to surface contact shows a decrease in velocity. Again, without slip the transition should be smooth, resulting in a velocity of zero at the contact point. If slip is present, the velocity curve intercepts the velocity axis ($D = 0$) at a finite value, which is easier to distinguish than a kink in the force curve.

The results depend on the molecular weight (Fig. 4). For 2.5 kDa PI the fit showed good agreement with the measurement up to the highest approaching velocity of 5 μm/s. This corresponds to $\eta v_0 = 3.5 \times 10^{-6}$ N/m. The slip lengths required to obtain the best fit were 5–10 nm, independent of the approaching velocity. Slip was not directly visible from the measured curves. It was also not visible in the velocity curve.

For 4.8 kDa PI the curves could not be fitted with any hydrodynamic model if we used bulk viscosities. To obtain a reasonable agreement between simulated and experimental curves, a viscosity of 4.0 Pa s had to be assumed, which is more than twice as high as the experimentally determined value. An increased viscosity of confined polymer melts has been observed with the SFA as well [10,15,50]. Also the pressure increase in the gap between microsphere and planar surface, which can reach ≈1000 bar, can increase the viscosity. Since the shear rates in the center of the gap between particle and surface are zero (this is discussed in detail later when also shear rate profiles are calculated), the confinement effect might be dominating for our experiments. For example, the zero shear viscosity of PDMS increases by one order of magnitude when increasing the pressure by ≈700 bar [57]. It might also be an indication that hydrodynamic forces in melts have to be described by a full viscoelastic theory.

Slip is evidently identified by a kink in the force curves at the contact point. It becomes even more evident in the velocity curves. For $D \to 0$ the velocity still possesses a finite value. Slip lengths decreased from 100 nm for 200 nm/s approaching speed, to 30 nm for 5000 nm/s approaching speed.

High molecular weight PI ($M_W = 10.2$ kDa) force curves could again be fitted with a hydrodynamic force including slip, up to values of ηv_0 of 8.0×10^{-6} N/m. Slip lengths of 30–80 nm were found, again independent on the approaching velocity. Slip was visible in force curves and in velocity curves.

3.2.2. Poly(dimethylsiloxane)

For comparison we also studied the hydrodynamic interaction in PDMS of different molecular weight (Fig. 5). PDMS spreads on silicon wafers and the contact angle is close to zero, indicating that the interaction between the polymer and the solid surface is even stronger than for PI. PDMS of a relatively high molecular weight ($M_W = 18.8$ kDa) could indeed

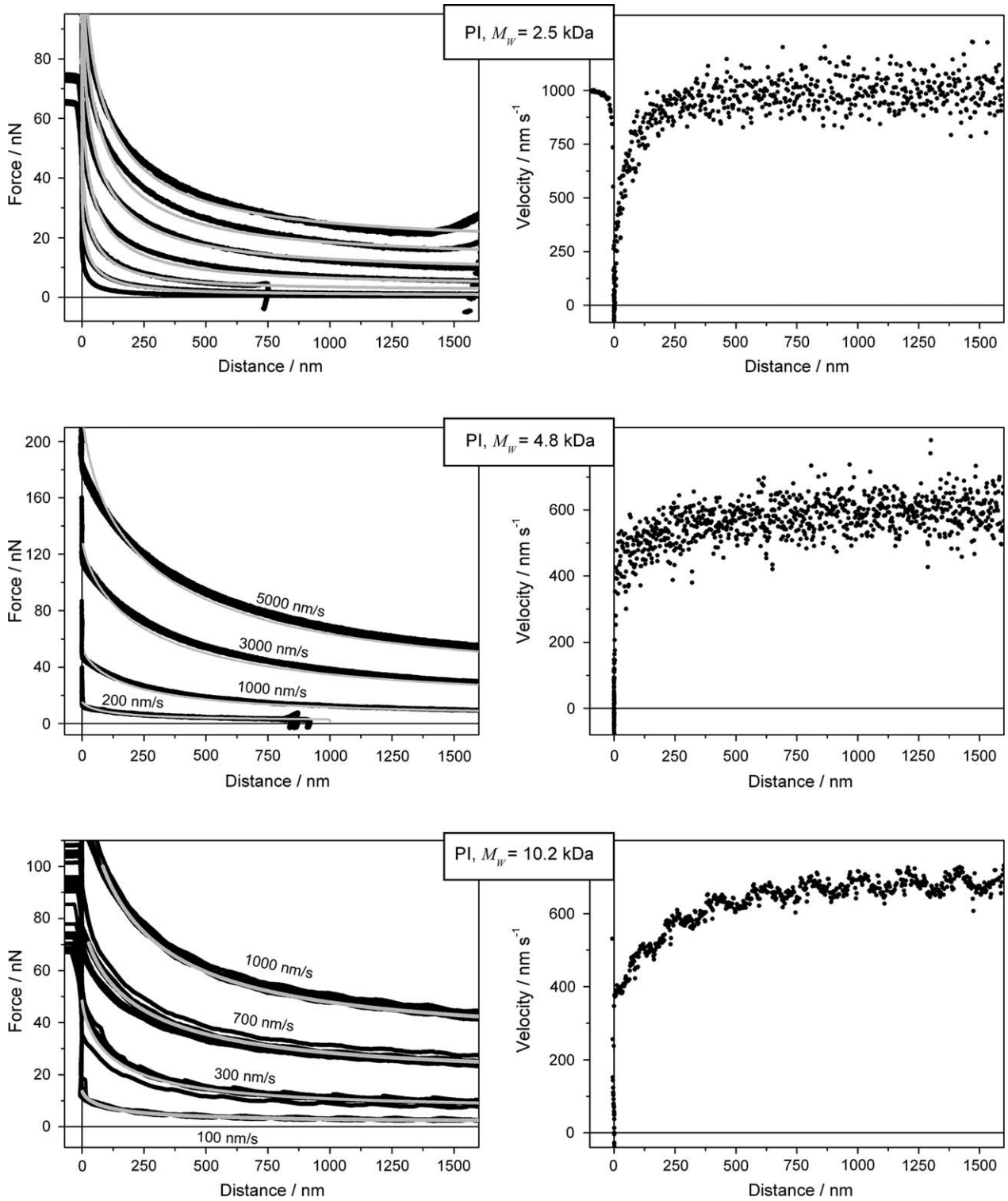

Fig. 4. Hydrodynamic force (left) and velocity (right) curves measured on silicon wafers with glass microspheres at different approaching velocities in PI. Only approaching parts are shown. The experimental results (●) are fitted by a hydrodynamic simulations including slip (gray lines). Top: PI of $M_W = 2.5$ kDa, $k_c = 0.27$ N/m, $R = 10.8$ μm, $\eta = 0.7$ Pa s at approaching velocities $v_0 = 0.2$, 0.5, 1, 2, 3, 4, and 5 μm/s (bottom to top curve). The velocity curve was recorded at $v_0 = 1000$ nm/s. Middle: PI of $M_W = 4.8$ kDa, $k_c = 0.26$ N/m, $R = 11.0$ μm, $\eta = 4.0$ Pa s at approaching velocities $v_0 = 0.2$, 1, 3, and 5 μm/s. The velocity curve was recorded at $v_0 = 600$ nm/s. Bottom: PI with $M_W = 10.2$ kDa, $k_c = 0.27$ N/m, $R = 10.8$ μm, $\eta = 7.7$ Pa s, $v_0 = 0.1$, 0.3, 0.7, and 1 μm/s. The velocity curve was recorded at $v_0 = 700$ nm/s.

be described by Eqs. (2) and (6) without assuming slip. Neither in the force curves nor in the velocity curves was any indication of slip. The fits showed good agreement up to $v_0 = 5$ μm/s, which corresponds to $\eta v_0 = 1.8 \times 10^{-6}$ N/m. For $v_0 = 10$ μm/s, the experimental curve diverged to higher forces (Fig. 5).

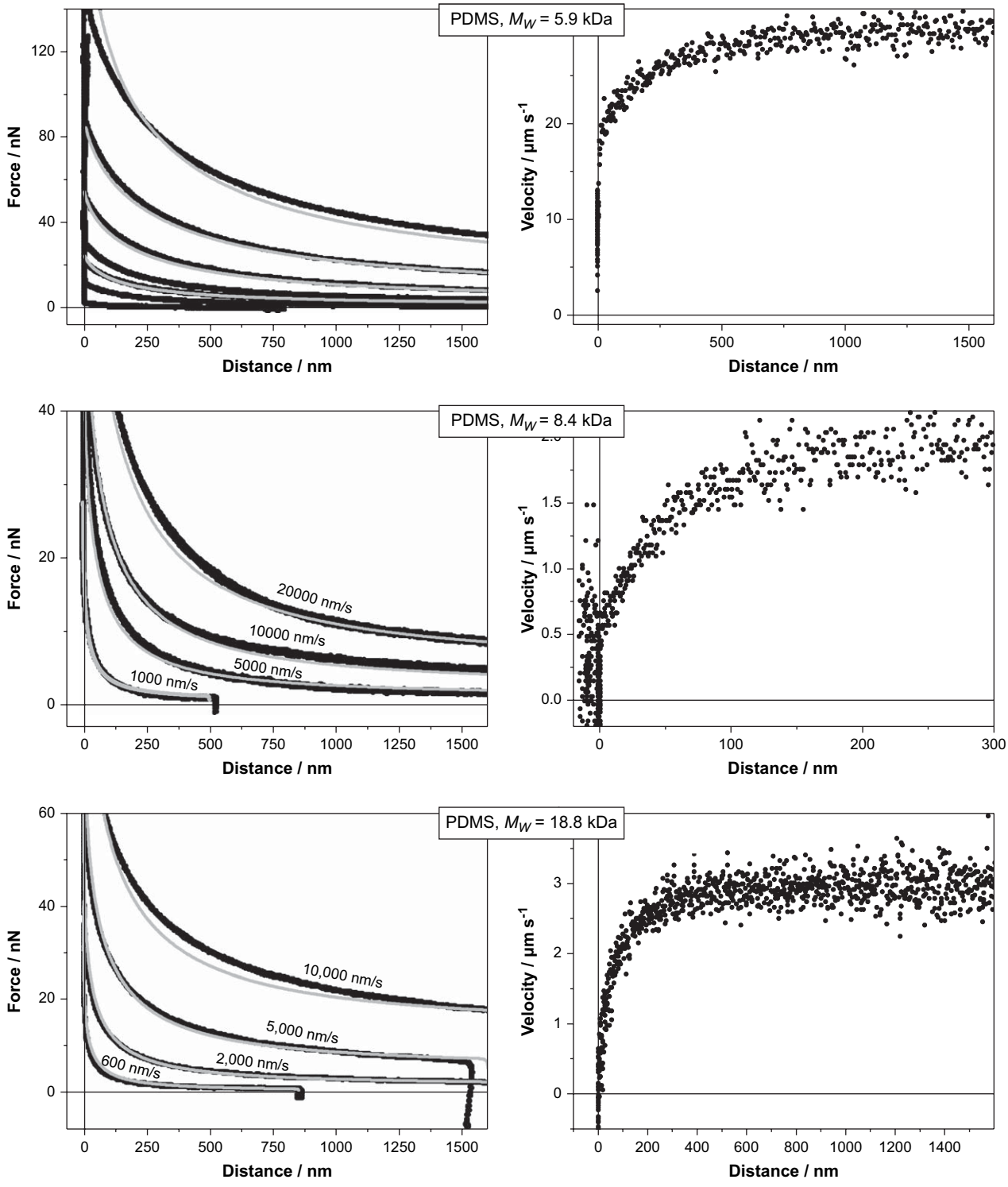

Fig. 5. Hydrodynamic force curves measured on silicon wafers with glass microspheres at different approaching velocities in poly(dimethylsiloxane) (PDMS). Only approaching parts are shown. Top: PDMS of $M_W = 5.9$ kDa, $k_c = 19$ N/m, $R = 9.1$ μm and $\eta = 0.22$ Pa s at approaching velocities $v_0 = 1$, 2, 5, 10, 15, 30, 60, and 100 μm/s (bottom to top curve). Middle: PDMS with $M_W = 8.4$ kDa, $k_c = 0.27$ N/m, $R = 11.0$ μm and $\eta = 0.15$ Pa s at $v_0 = 1$, 5, 10, and 20 μm/s. Bottom: PDMS of $M_W = 18.8$ kDa, $k_c = 0.24$ N/m, $R = 10.8$ μm and $\eta = 0.36$ Pa s at approaching velocities $v_0 = 0.6$, 2, 5, and 10 μm/s. The experimental results (●) are fitted by hydrodynamic simulations without slip (gray lines).

For a molecular weight of $M_W = 8.4$ kDa the force curves did not show slip, velocity curves did. In contrast to higher molecular weights, the force curves could only be fitted assuming a viscosity of 0.15 Pa s, which was three times larger then experimental values, and no slip. The fits were in good agreement up to 20 μm/s, which corresponds to $\eta v_0 = 3.0 \times 10^{-6}$ N/m.

PDMS of low molecular weight ($M_W = 5.9$ kDa) could only be fitted with a viscosity of 0.22 Pa s which is four times higher than the bulk viscosity and a slip of 70 nm. Slip was

obvious in force curves and velocity curves, but like for PI of 4.8 kDa and PDMS of 8.4 kDa, the viscosity had to be increased by a factor of 2–4 to get agreement between experimental and simulated curves. Assuming increased viscosity, fitting was possible up to 60 μm/s ($\eta v_0 = 132 \times 10^{-6}$ N/m). For 100 μm/s the experimental curve diverged to higher forces.

3.2.3. Possible artifacts

Before we discuss the slip occurring in most experiments we estimate the effect of possible artifacts. Several sources of possible misinterpretation of hydrodynamic force experiments have been identified. We rule out two, identify a third possible artifact, and eventually argue that in our case it is insignificant.

Surface asperities can lead to apparent slip. If a surface asperity is preventing the sphere and planar surface to approach closer than a certain distance, the zero distance would not be identical to the real (or average) distance. This could in principle cause an apparent slip by limiting the distance of closest approach. To verify that asperities did not significantly influence the results we imaged the particles with a grid of asperities as described in Refs. [58–60] and imaged the substrates with an AFM. In our experiments the substrate used and the particle surface were smooth and showed no asperities. Measured RMS roughnesses over 1 μm^2 on sphere and flat surface were typically 0.27 nm for the surface and 4 nm for the sphere as determined by AFM imaging (Fig. 6).

Another possible source of apparent slip is the distance-dependent hydrodynamic force on the cantilever, without consideration of the sphere. In particular for tilted cantilevers the end of the cantilever might contribute with a distance-dependent component [56,61]. For the microspheres and cantilevers used here this force can be considered constant. For typical values ($R = 10$ μm, $v_0 = 5$ μm/s, $k_c = 0.26$ N/m, $L = 120$ μm, $w = 36$ μm, $\eta = 0.6$ Pa s) the force is 0.47 nN for $D = 0$ and

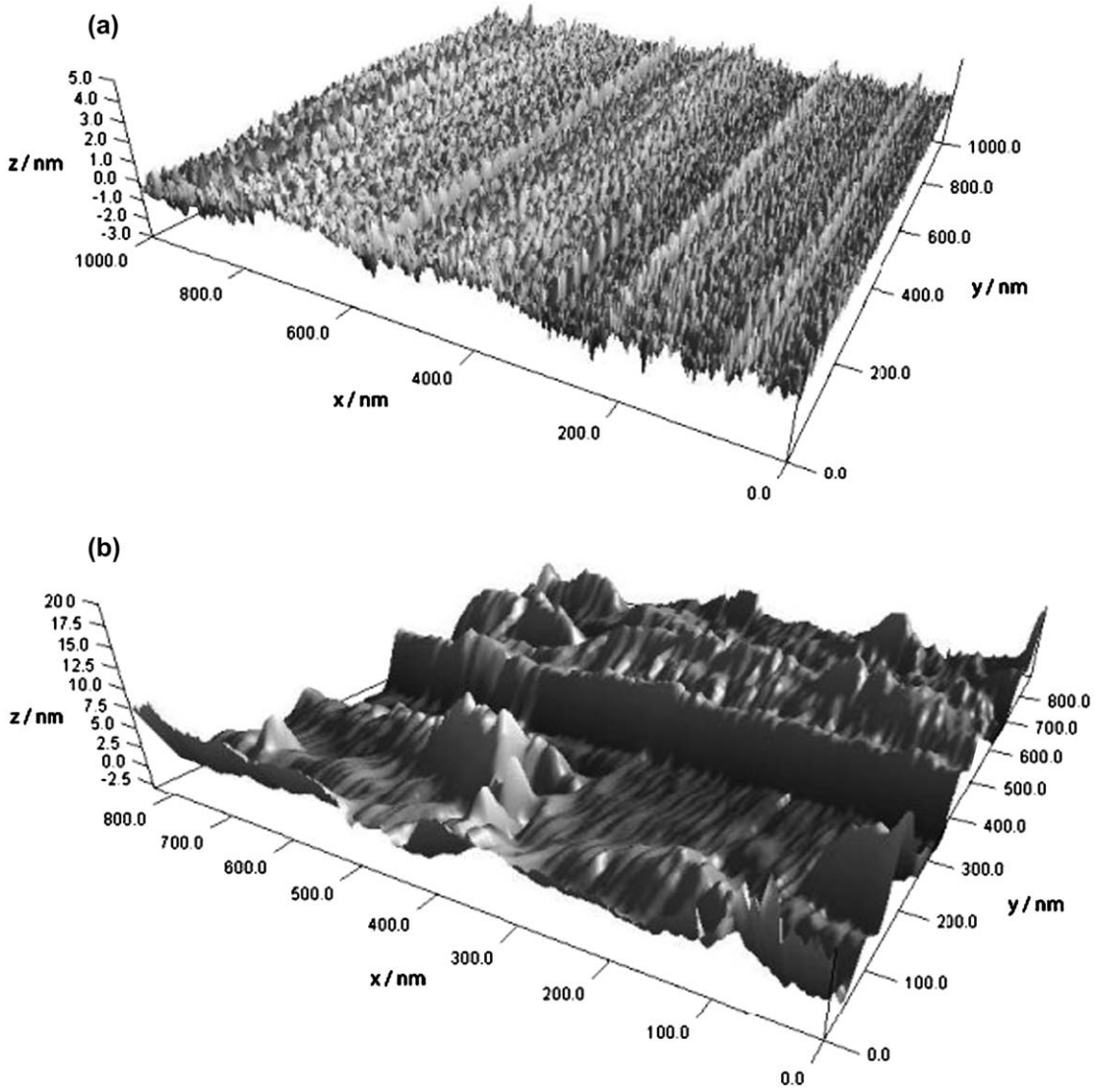

Fig. 6. AFM images of (a) a silicon wafer and (b) a particle on the cantilever. The particle was imaged with a μmasch tip characterization grid TGT01 (Anfatec, Oelsnitz, Germany) with tip curvature radii of less than 10 nm, a height of 0.3–0.6 nm and a distance of 2.12 μm between the tips.

0.42 nN for $D = 1$ μm. Compared to the hydrodynamic force on the particle this change is negligible.

A third effect might, however, change the shape of hydrodynamic force curves. Since to our knowledge it was not described in the literature yet, we describe it in detail here. When the microsphere approaches the planar surface its velocity is gradually reduced until it reduces to zero. This does not only reduce the hydrodynamic drag on the microsphere, but on the cantilever as well. Different parts of the cantilever are differently affected. The base of the cantilever, close to the chip, is only weakly affected because it moves with a velocity close to v_0. The end of the cantilever, where the microsphere is attached and which dominates the total interaction [61], is strongly affected because here the velocity reduction is significant. To quantify this effect we replaced the constant hydrodynamic force term in Eq. (6) by

$$F_{\text{drag}} = \alpha \frac{1}{v_0}\left|\frac{\mathrm{d}D}{\mathrm{d}t}\right| F_0 + (1-\alpha)F_0 \tag{9}$$

Here, F_0 is the drag on the cantilever acting if all parts are moving with v_0 and α is the proportion contributed by the end of the cantilever. Hydrodynamic force curves simulated with Eq. (9) are indeed influenced by the drag force on the cantilever (Fig. 7). This influence is, however, small. The effect of slip will dominate. Only for slip lengths $b < 10$ nm the influence should be considered.

3.2.4. Slip

Discussing the presence of slip and considering even all these possible sources of misinterpretation the experiments indicate slip in all cases with the exception of PDMS $M_W = 18.8$ kDa. In most cases slip is directly evident (PI $M_W = 4.8$ kDa, PI $M_W = 10.2$ kDa, PDMS $M_W = 5.9$ kDa), in other cases only the fit required slip (PI $M_W = 2.5$ kDa, PDMS $M_W = 8.4$ kDa). There are three different ways to interpret apparent slip:

1. The velocity of the polymer melt at the solid surface or in a shear plane close to the solid surface is not zero and a freely moving melt is sliding over the solid surface or over a layer bound to the solid.

2. The viscosity of the melt close to the solid surface is reduced with respect to its bulk viscosity so that a steeper velocity gradient arises. An explanation for this could be shear thinning: The flow of the melt aligns the linear polymer chains and reduces the effective viscosity.

3. AFM force measurements do not allow to determine the absolute value for zero distance between sphere and surface. Zero distance is assumed when the sphere stops moving, which is when hard contact is attained. It could happen that the normal pressure of the tip induces a phase change in the polymer so that it solidifies abruptly and the tip cannot further penetrate. The polymer forms a solid surface layer and the "zero distance" measured by the AFM is instead several tenths of nanometers from the solid surface. To avoid confusion we would like to stress the difference to the immobilized layer mentioned earlier: The immobilized layer is always present while a "solidifying" layer forms abruptly at approach. If a solid layer is formed, it should be possible to fit the force curves by simply shifting the simulated curves by the thickness of the layer. This is attained by substituting the distance D in Eq. (3) with a modified distance $\Delta D = D_L + D$, with D_L being the thickness of the solidified polymer layer, and then simulating the curve as usual. The two different models ("slip length" and "curve shift") are both valid for correctly fitting the force curves, so that we are not able to discriminate between them. On the other hand we are able to discriminate between the two models in a velocity curve. Two factors play a role: The steepness of the velocity-versus-distance curve decreases close to the surface, and the contact velocity at $D = 0$. Very close to the surface (<5 nm), the experiment agrees with the slip model. The contact velocities of the slip model and of the experiment are similar (Fig. 8), while the no-slip model and the curve shift model cannot account for both: the shape of the experimental curve and the contact velocity. It should be noted that even though the fits support the slip model, the differences are too weak to allow ruling out completely the existence of a solidifying layer on the surface.

A typical profile of shear rates in the gap between particle and surface shows highest shear rates at a circle around the center of approach (Fig. 9). This profile depends on the distance of the particle and surface and, assuming no slip, maximum shear rates approach infinity, for $D \to 0$. To calculate maximal shear rates during the approach of the particle, we used [40]

$$\dot{\gamma}_{\max} = \frac{9\sqrt{2R}}{D^{2/3}\sqrt{3R}}\frac{\mathrm{d}D}{\mathrm{d}t} \tag{10}$$

This equation was developed for Newtonian liquids, where the velocity dD/dt depends linearly on the viscosity. It is not strictly valid in our experiments with polymers, where the

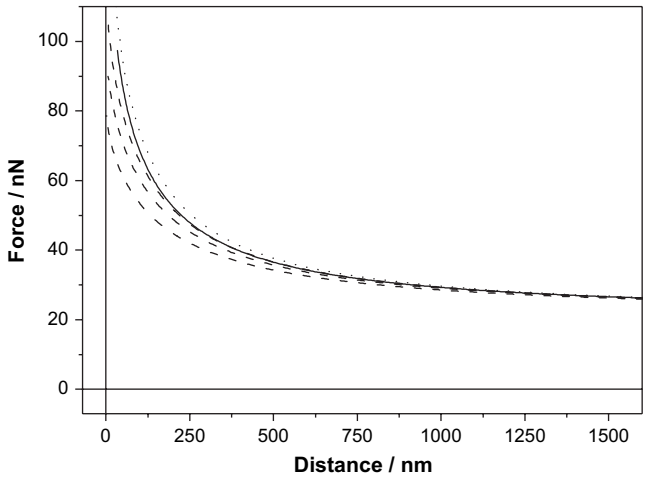

Fig. 7. Hydrodynamic force curves simulated with $R = 10$ μm, $v_0 = 5$ μm/s, $k_c = 0.26$ N/m, $L = 120$ μm, $w = 36$ μm, $\eta = 0.6$ Pa s, and $F_{\text{drag}} = 13$ nN for no slip (dotted), no slip and taking the varying drag on the cantilever into account according to Eq. (10) with $\alpha = 1$ and $F_0 = 13$ nN (continuous line), and slip of $b = 20$, 40, and 80 nm (dashed, from top to bottom). For the dashed curves $F_{\text{drag}} = 13$ nN and $\alpha = 0$.

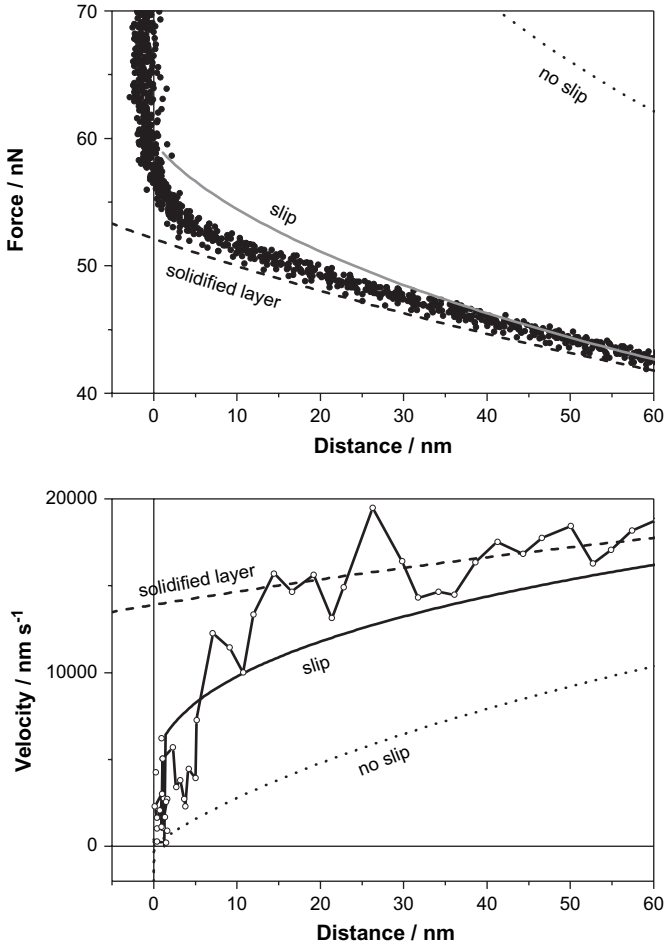

Fig. 8. Velocity curve (below) and force curve (above) for 5.9 kDa PDMS, $v_0 = 30$ μm/s, $R = 9.1$ μm, $k_c = 0.19$ N/m, $\eta = 0.22$ Pa s. The experimental data (below: lines and dots, above: dots) has been fitted assuming no slip (dots), assuming slip (line), and assuming a solid layer on the surface (dashed).

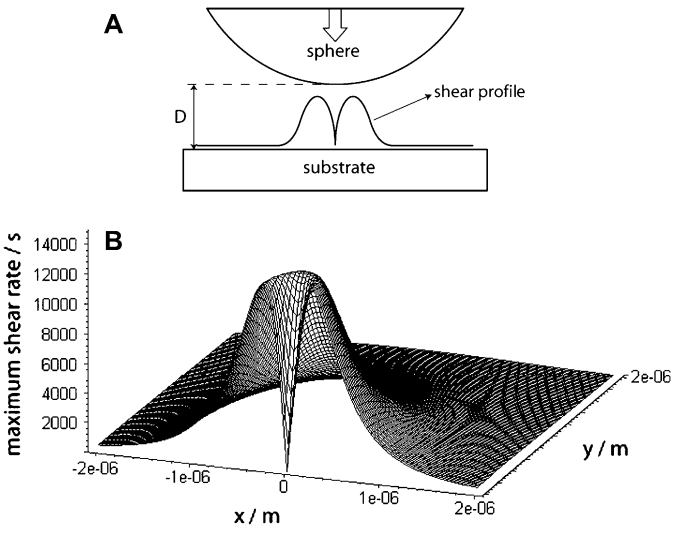

Fig. 9. A: A scheme of a shear rate profile is shown as a vertical cut through the surface. The tip approaches the surface, and the maximum shear rates are reached at a circle around the contact area. B: Simulated maximum shear rates for $\eta = 0.05$ Pa s, $R = 10$ μm, $v_0 = 30$ μm/s, $D = 10$ nm, without slip. The shear rates are plotted versus the lateral distance on the surface.

viscosity might not be constant, but it can provide an estimation of occurring shear rates. To compare the force experiments, shear rates at a fixed distance $D = 10$ nm for $R = 10$ μm, $k_c = 0.27$, and $b = 0$ were calculated with Eq. (10) for each polymer at all measured velocities. Maximal shear rates were up to 2.5×10^5 s^{-1} for 5.9 kDa PDMS, 8×10^4 s^{-1} for 8.4 kDa PDMS, 3×10^4 s^{-1} for 18.8 kDa PDMS, 1.5×10^4 s^{-1} for 2.5 kDa PI, 10^4 s^{-1} for 4.8 kDa PI, and 2×10^3 s^{-1} for 10.2 kDa PI.

4. Conclusions

Surface interactions on different surfaces across PI were measured in quasi-static and hydrodynamic experiments. Quasi-static measurements showed almost no force compared to earlier measurements in PDMS, implying that no or only a thin immobilized surface layer is formed in PI. This confirms theoretical predictions. As a second approach, the occurrence of slip was measured in hydrodynamic experiments. Slip occurred for those polymers, which in quasi-static experiments showed a weak or even attractive force (PI and low molecular weight PDMS). No slip was observed with high molecular weight PDMS, which in quasi-static experiments showed a strong repulsion, indicating the presence of an immobilized layer.

Acknowledgements

We acknowledge the German Research Foundation DFG Bu 701/21 for the financial support, T. Wagner and J. Thiel for the synthesis of the polymers, A. Hanewald for the viscosity measurements and M. Wagner for the NMR measurements.

References

[1] de Gennes PG. CR Acad Sci Paris 1987;305:1181.
[2] Ausserré D. J Phys (Paris) 1989;50:3021.
[3] Subbotin A, Semenov A, Hadziioannou G, ten Brinke G. Macromolecules 1996;29:1296.
[4] Müller M, Albano EV, Binder K. Phys Rev E 2000;62:5281.
[5] Leermakers FAM, Butt H-J. Phys Rev E 2005;72:021807.
[6] ten Brinke G, Ausserre D, Hadziioannou G. J Chem Phys 1988;89:4374.
[7] Thompson PA, Grest GS, Robbins MO. Phys Rev Lett 1992;68:3448.
[8] Horn RG, Hirz SJ, Hadziioannou G, Frank CW, Catala JM. J Chem Phys 1989;90:6767.
[9] van Alsten J, Granick S. Macromolecules 1990;23:4856.
[10] Montfort JP, Hadziioannou G. J Chem Phys 1988;88:7187.
[11] Hirz SJ, Homola AM, Hadziioannou G, Frank CW. Langmuir 1992;8:328.
[12] Hirz S, Subbotin A, Frank C, Hadziioannou G. Macromolecules 1996;29:3970.
[13] Ruths M, Granick S. J Phys Chem B 1999;103:8711.
[14] Israelachvili JN, Kott SJ. J Chem Phys 1988;88:7162.
[15] Luengo G, Schmitt FJ, Hill R, Israelachvili J. Macromolecules 1997;30:2482.
[16] Georges JM, Millot S, Loubet JL, Tonck A. J Chem Phys 1993;98:7345.
[17] Hu HW, Granick S. Science 1992;258:1339.
[18] Hu HW, Granick S, Schweizer KS. J Non-Cryst Solids 1994;172–174:721.
[19] Peanasky J, Cai LL, Granick S, Kessel CR. Langmuir 1994;10:3874.
[20] Horn RG, Israelachvili JN. Macromolecules 1988;21:2836.

[21] Horn RG, Smith DT, Haller W. Chem Phys Lett 1989;162:404.
[22] Sun G, Kappl M, Butt H-J. Eur Polym J 2005;41:663.
[23] Sun G, Kappl M, Pakula T, Kremer K, Butt H-J. Langmuir 2004;20:8030.
[24] Sun G, Kappl M, Butt H-J. Colloids Surf A 2004;250:203.
[25] Homola AM, Nguyen HV, Hadziioannou G. J Chem Phys 1991;94:2346.
[26] Campbell SE, Luengo G, Srdanov VI, Wudl F, Israelachvili JN. Nature 1996;382:520.
[27] Yu C, Evmenenko G, Kmetko J, Dutta P. Langmuir 2003;19:9558.
[28] Fetters LJ, Lohse DJ, Milner ST, Graessley WW. Macromolecules 1999;32:6847.
[29] de Gennes PG. Macromolecules 1982;15:492.
[30] Scheutjens JMHM, Fleer GJ. Macromolecules 1985;18:1882.
[31] Granick S, Hu HW. Langmuir 1994;10:3857.
[32] Evmenenko G, Mo H, Kewalramani S, Dutta P. Polymer 2006;47:878.
[33] Benbow JJ, Lamb P. SPE Trans 1963;3:7.
[34] Vinogradov GV, Froishteter GB, Trilisky KK. Rheol Acta 1978;17:156.
[35] Mashelkar RA, Dutta A. Chem Eng Sci 1982;37:969.
[36] Denn MM. Annu Rev Fluid Mech 1990;22:13.
[37] Wang SQ, Drda PA. Macromolecules 1996;29:2627.
[38] Mhetar V, Archer LA. Macromolecules 1998;31:8607.
[39] Yang X, Ishida H, Wang SQ. J Rheol 1998;42:63.
[40] Horn RG, Vinogradova OI, Mackay ME, Phan-Thien N. J Chem Phys 2000;112:6424.
[41] Léger L. J Phys Condens Matter 2003;15:S19.
[42] Brochard F, de Gennes PG. Langmuir 1992;8:3033.
[43] Hatzkiriakos SG, Kalogerakis N. Rheol Acta 1994;33:38.
[44] Hill DA. J Rheol 1998;42:581.
[45] Yarin X, Graham MD. J Rheol 1998;42:1419.
[46] Joshi YM, Lele AK, Mashelkar RA. J Non-Newtonian Fluid Mech 2000; 94:135.
[47] Inn Y, Wang SQ. Phys Rev Lett 1996;76:467.
[48] Litvinov VM, Zhdanov AA. Polym Sci USSR 1987;29:1133.
[49] Litvinov VM, Barthel H, Weis J. Macromolecules 2002;35:4356.
[50] Hartmann L, Kremer F, Pouret P, Léger L. J Chem Phys 2003; 118:6052.
[51] Hutter JL, Bechhoefer J. Rev Sci Instrum 1993;64:1868.
[52] Butt H-J, Jaschke M. Nanotechnology 1995;6:1.
[53] Brenner H. Chem Eng Sci 1961;16:242.
[54] Chan DYC, Horn RG. J Chem Phys 1985;83:5311.
[55] Vinogradova OI. Langmuir 1995;11:2213.
[56] Vinogradova OI, Butt H-J, Yakubov GE, Feuillebois F. Rev Sci Instrum 2001;72:2330.
[57] Mertsch R, Wolf BA. Macromolecules 1994;27:3289.
[58] Siedle P, Butt H-J, Bamberg E, Wang DN, Kühlbrandt W, Zach J, et al. Inst Phys Conf Ser 1992;130:361.
[59] Vesenka J, Miller R, Henderson E. Rev Sci Instrum 1994;65:2249.
[60] Neto C, Craig VSJ. Langmuir 2001;17:2097.
[61] Vinogradova OI, Yakubov GE. Langmuir 2003;19:1227.